Bio-Design and Manufacturing (2025) 8:909–916
https://doi.org/10.1631/bdm.2500186

TECHNICAL NOTE

Automated device for small-tissue extraction and primary organoid modeling

Wanlong Wang[1,2] · Yongde Cai[1,2] · Davit Khutsishvili[1] · Xiaoyong Dai[1,2] · Yifu Wei[2] · Zhiyuan Liu[2] · Yu Zhu[1] · Zitian Wang[1] · Shaohua Ma[1,2]

Received: 14 April 2025 / Accepted: 9 June 2025 / Published online: 15 July 2025

Graphical abstract

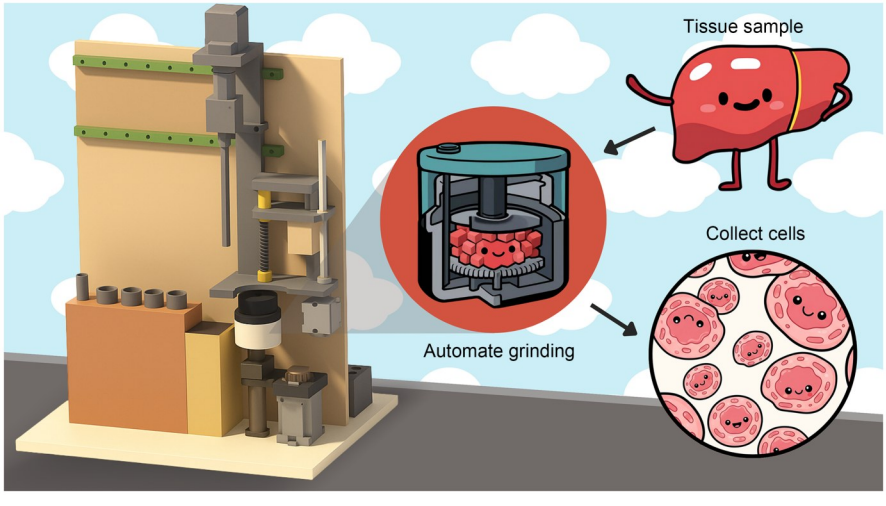

We developed a small-tissue extraction device (sTED), an automated system that integrates 1-min mechanical dissociation and enzymatic digestion to extract viable primary cells from ultrasmall tissue samples (5–20 mg) within 10 min. Unlike conventional methods, sTED minimizes cell loss and enhances reproducibility, achieving >90% cell viability in mouse tissues and >60% in human tumors, with 1.5×10^4–2.5×10^4 cells/mg yield from mouse liver. Tailored for biopsies and ultrasmall samples, sTED addresses critical standardization challenges in organoid-based research.

✉ Shaohua Ma
ma.shaohua@sz.tsinghua.edu.cn

[1] Institute of Biopharmaceutical and Health Engineering, Tsinghua Shenzhen International Graduate School (SIGS), Tsinghua University, Shenzhen 518055, China

[2] SynOrg Biotechnology (Shenzhen) Co., Ltd., Shenzhen 518107, China

1 Introduction

Organoid models derived from primary tissues have emerged as a powerful tool in precision medicine, integrating the strengths of human genetics with rapid modeling and compatibility with gene editing techniques [1, 2]. These models are particularly promising for personalized medicine applications [3, 4], including tumor modeling [5–8], immune studies [9, 10], and metabolic research [11], among others [12, 13]. However, their success depends on the efficient extraction of viable primary cells, a process that remains challenging to standardize.

Current approaches, combining enzymatic digestion with manual tissue grinding, face notable limitations. Standardization is hindered by the need for repeated optimization of digestion time, enzyme concentration, and manual handling [14]. Inadequate cutting impairs enzymatic digestion and reduces cell yield [15], whereas excessive cutting increases cell necrosis [16]. Transfer-related cell loss is

particularly pronounced in ultrasmall samples, and expansion techniques are time-consuming and may alter cell properties.

Commercial instruments, such as Singleron's PythoN® System, Miltenyi's gentleMACS™ Dissociator, and TissueGrinder, are optimized for large tissue specimens and require approximately 0.5 h per sample [17]. Yet, clinical data reveal that over 70% of samples are biopsies, often ultrasmall tissues (5–20 mg) [18, 19], emphasizing the demand for methods tailored to limited sample sizes. The sTED system eliminates tissue transfer steps, completes mechanical dissociation in 1 min, and achieves full extraction within 10 min, offering superior consistency and cell viability compared to conventional approaches, particularly for ultrasmall samples.

2 Workflow

The sTED system (Fig. 1a) comprises four integrated modules: a grinding module, a temperature control module, a pressure adjustment module, and an injection module (Fig. 1b). Its standard workflow streamlines the dissociation of primary tissues into viable single-cell suspensions through an automated, temperature-controlled process (Fig. 1c). Reagents were prepared before device operation as follows:

(1) Wash buffer: To prepare 25 mL of wash buffer, 24.75 mL of Dulbecco's modified Eagle medium (DMEM)/F12 reagent was mixed with 250 μL of penicillin–streptomycin solution (P/S reagent).

(2) 10× digestion solution: To prepare the digestion solution, 200 mg each of collagenase IV, III, and I, and dispase, along with 13.33 mg of deoxyribonuclease I (DNase I), were dissolved in 10 mL of Dulbecco's phosphate-buffered saline (DPBS) solution. The solution was vortexed thoroughly to ensure complete dissolution and sterilized by filtration through a 0.22-μm membrane filter. The digestion solution was prewarmed to 37 °C before use.

(3) Serum-containing medium: To prepare 6 mL of serum-containing medium, 5.4 mL of wash buffer was mixed with 600 μL of fetal bovine serum.

Tissue samples and equipment were prepared as follows: The grinding plate was installed inside a grinding chamber, and then the grinding chamber was mounted onto the equipment. Next, the freshly harvested tissue was manually trimmed into approximately 1 cm^3 pieces and loaded into the grinding chamber, followed by the addition of 3 mL of pre-chilled grinding buffer at 4 °C. Three 15-mL centrifuge tubes were installed from left to right in the injection module, along with one 50-mL centrifuge tube. A 100-μm cell filter was placed on the 50-mL centrifuge tube, and a 5-mL pipette tip was attached to the far right. The 15-mL centrifuge tubes were numbered 1, 2, and 3 (Fig. 1g). Then, 12 mL of wash buffer was added to centrifuge tube 1, 600 μL of 10× digestion solution was added to centrifuge tube 2, and 6 mL of stop digestion solution was added to centrifuge tube 3.

After the device power and data transfer cables were connected, the relevant program on the computer was opened, and the "Start" option was clicked.

Upon activation, the device automatically lowered the upper grinding head to the preset grinding height, initiating mechanical dissociation. For most soft tissue types, the initial grinding step was completed within 1 min. Immediately after this step, a concentrated digestive enzyme solution was introduced into the chamber via the injection module. Simultaneously, the temperature control module increased the chamber temperature to 37 °C, the optimal temperature for enzymatic activity. The entire process, illustrated in Fig. 1c, integrates seamlessly with the modular architecture of sTED (Figs. 1d–1h).

Throughout the enzymatic digestion phase, the grinding module continued to operate in a coordinated stirring mode. By cyclically separating and rotating the grinding surfaces, the system generated dynamic shear and mixing conditions, promoting the uniform exposure of tissue fragments to the enzymes and preventing sedimentation. After the completion of the primary digestion cycle, the injection module delivered an additional volume of digestion solution to finalize the enzymatic breakdown of tissue. The resulting cell suspension was then automatically dispensed onto a built-in filter screen, which retained undigested tissue debris and allowed single cells to pass through.

The filtrate was centrifuged at 300*g* for 5 min. The resulting supernatant was discarded, and the pellet was resuspended in 3 mL of red blood cell lysis buffer and incubated for 2 min at room temperature. A second centrifugation was performed at 300*g* for 5 min, and the final pellet was resuspended in culture medium for downstream applications.

3 Experimental methods

3.1 Manual primary cell extraction

Tissues were rinsed three times with DPBS and minced on ice into approximately 1 mm^3 fragments using sterile scissors. Fragments were transferred to a 15-mL tube using a cut 1-mL pipette tip, mixed with 5–8 mL of wash buffer and pre-warmed 10× digestion solution, and incubated at 37 °C for 5 min (liver tissue). The suspension was filtered through a 100-μm strainer, washed with buffer, and centrifuged at 300*g* for 5 min. The pellet was resuspended in 5 mL of red blood cell lysis buffer for 2 min at room temperature, centrifuged again at 300*g* for 5 min, and resuspended in culture medium.

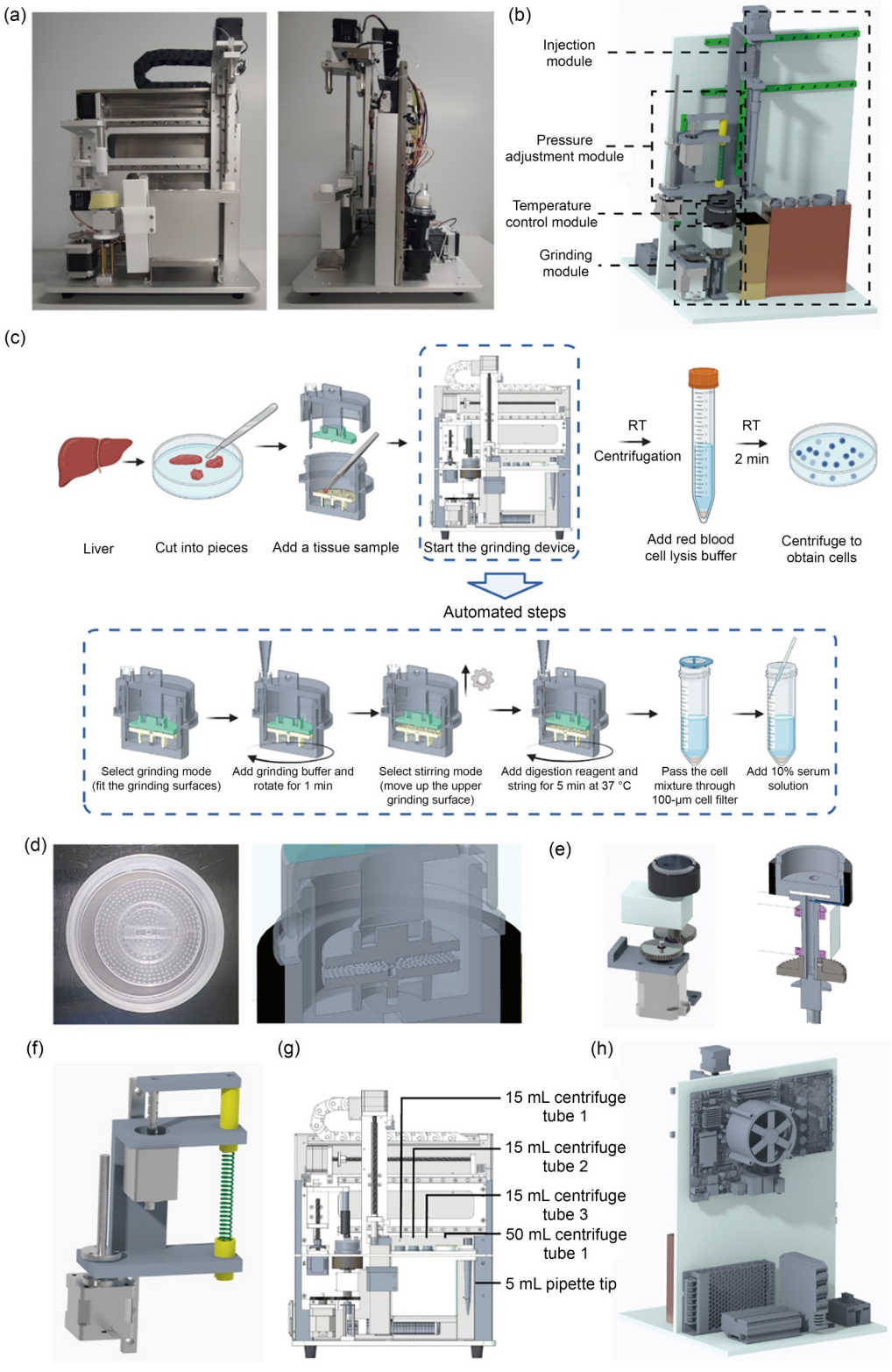

Fig. 1 Small-tissue extraction device (sTED). (a) Photographs of the prototype. (b) Three-dimensional model illustrating the following module functions: The pressure adjustment module utilizes a mechanical pressure regulator to vary the tissue grinding pressure; the temperature control module, equipped with a thermosensor and heating resistors, maintains the grinding chamber temperature; the grinding module features a motor-driven lower grinding sheet and an upper grinding sheet that applies pressure for continuous tissue cutting; the injection module is designed for fluid addition via removable syringes. (c) Flowchart showing the cell extraction process. Detailed images of the device components, including the grinding module (d), temperature control module (e), pressure adjustment module (f), and injection module (g), with the power supply and microcontroller (h). RT: room temperature

3.2 Singleron PythoN primary cell extraction

Tissues were rinsed in DPBS, cut into approximately 1 cm^3 pieces, and placed in dissociation tubes. A mixture of 500 μL of 10× digestion solution and 4.5 mL of wash buffer (98% DMEM/F12+2% P/S) was added. Tubes were sealed, processed on Singleron PythoN for 35 min, filtered through a 100-μm strainer, centrifuged at 300*g* for 5 min, treated with red blood cell lysis buffer for 2 min, and centrifuged again at 300*g* for 5 min.

3.3 Parameter optimization

Using mouse liver tissue, grinding temperature (4 to 37 °C), rotation speed (60 r/min), pressure (1 N), grinding time (1 min), and digestion time (5 min) were tested. Cell yield and viability were measured with Calcein acetoxymethyl ester/propidium iodide (Calcein AM/PI) staining and automated counting. Temperature stability was monitored over six replicates.

3.4 Cell extraction efficiency

The efficiency of sTED, manual, and commercial methods (Singleron, TissueGrinder) was compared. Viability was assessed using Calcein AM/PI staining (1 μmol/L Calcein AM, 5 μmol/L PI, 15 min at 37 °C), and yield was quantified per milligram of input tissue.

3.5 Surgical tissue size evaluation

Ultrasmall (≤20 mg) and small (20–100 mg) samples from mouse liver, lung, and patient-derived organoid xenograft (PDOX) tumors were processed to compare yield, viability, and batch-to-batch variability under optimized sTED conditions.

3.6 Immunofluorescence staining

Dissociated cells were centrifuged onto glass slides at 300*g* for 5 min and allowed to settle for 5 min. Cells were fixed, stained, blocked, and permeabilized with 5% bovine serum albumin (BSA) and 0.1% Triton X-100 for 1 h. Slides were incubated with primary antibodies overnight at 4 °C, washed, incubated with fluorophore-conjugated secondary antibodies for 1 h at room temperature, washed again, stained with 4′,6-diamidino-2-phenylindole (DAPI) (5 μg/mL) for 15 min, and imaged.

3.7 Cell viability fluorescence staining

A Calcein AM/PI working solution (1 μmol/L Calcein AM, 5 μmol/L PI in DPBS, AM:PI:DPBS=1:3:1000) was prepared, and 100 μL was added to wells. Samples were incubated in the dark at 37 °C for 15 min, washed with DPBS, and imaged at 488 nm (Calcein AM) and 545 nm (PI).

4 Experimental results

4.1 Optimal parameters of sTED

To investigate the mechanical performance of the grinding module in the sTED system, we first compared two shear configurations, triangle-to-triangle (T–T) and triangle-to-square (T–S). As depicted in Fig. 2a, the T–S and T–T configurations achieved cell viability of >90% (Fig. 2b). However, under Calcein AM live-cell staining, the fluorescence of the T–S configuration was stronger, indicating greater cell activity and better cell condition (Fig. 2a). This improved outcome is attributed to the formation of a microblade array generated by the T–S interaction, which enables more efficient tissue shearing and also minimizes damage to cells. The sharper and asymmetric shear interface in the T–S configuration facilitates rapid tissue disaggregation and delicate cell handling, thereby increasing cell viability.

After optimizing the shear interface geometry, we used primary mouse liver tissue to evaluate the impact of key operational parameters on the overall extraction efficiency of sTED. In particular, we investigated the effects of grinding pressure, grinding temperature, grinding time, and digestion time.

As depicted in Fig. 2c, a grinding pressure of <1 N markedly decreased the cell yield, a mechanical pressure regulator module indicating that an adequate downward force is essential for effective tissue fragmentation. As shown in Fig. 2d, different grinding temperatures resulted in no significant differences in the final cell viability and yield. Considering that tissue preservation is typically performed at 4 °C, 4 °C was ultimately selected as the initial grinding temperature.

As depicted in Fig. 2e, reducing the grinding time to <1 min significantly impaired cell recovery, showing insufficient mechanical dissociation at shorter durations, whereas 1 min of operation represented the most efficient point in terms of cell extraction efficiency (right).

Figure 2f shows that digestion time was also a critical factor, wherein a short digestion period of 2 min was inadequate for enzyme activity, whereas extending the digestion time beyond 15 min negatively impacted the yield, probably due to overdigestion and cell degradation.

On the basis of these evaluations, we established the optimal extraction parameters for mouse liver tissue as follows: initial grinding temperature of 37 °C that gradually increases, rotation speed of 60 r/min, grinding pressure of 1 N, grinding time of 1 min, and digestion time of 5 min. These conditions provided a balance between enzymatic and mechanical processing, maximizing both viability and yield.

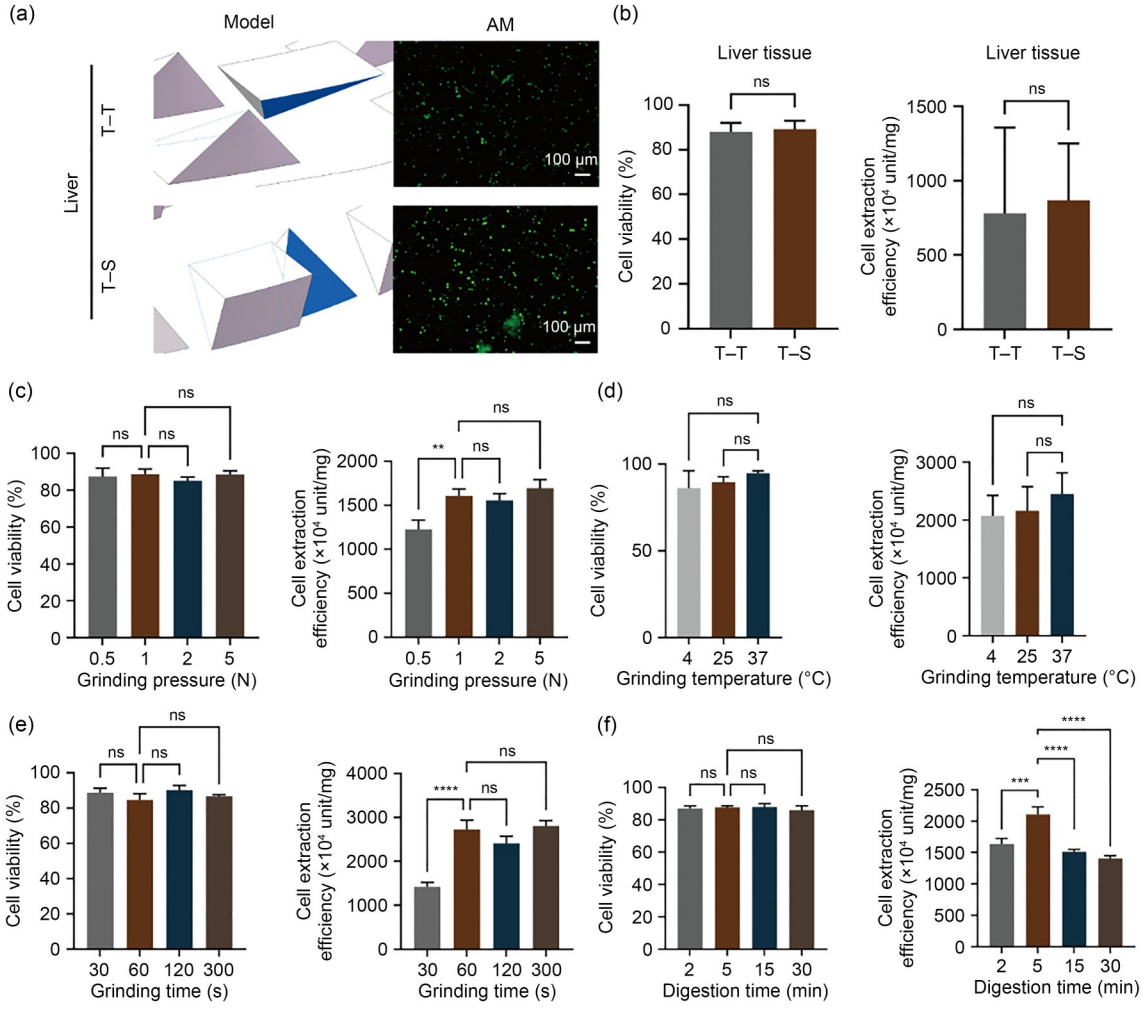

Fig. 2 sTED optimization. (a, b) A comparison of shear shapes shows the T–S and T–T configurations; T–S improved the shearing efficiency and reduced cell damage. Evaluation of the effects of varying grinding pressures (c), temperatures (d), grinding times (e), and digestion times (f) on cell viability (left) and unit mass extraction rates (right) in mouse liver tissue. Data are expressed as mean±standard deviation (n=4). $^{**}p<0.01$, $^{***}p<0.001$, and $^{****}p<0.0001$; ns: not significant

4.2 Primary cell extraction from normal tissue

We investigated the extraction efficiency of the sTED system using mouse liver and lung tissues and compared its performance with that of manual extraction using the Singleron's PythoN tissue dissociation system (Fig. 3). The important parameters evaluated in this experiment included cell viability, yield, and batch-to-batch variability.

For liver tissue extraction in both mice and rats, the cell viability was similar between sTED and Singleron (averaging approximately 89%), and both methods yielded higher results than the manual method. However, sTED resulted in a significantly higher cell yield per gram of tissue than manual extraction and the Singleron device. Overall, the higher efficiency of sTED provides a greater number of viable cells for downstream applications. Moreover, sTED achieved markedly lower batch-to-batch variability than the manual method, which demonstrated the greatest inconsistency in yield (Fig. 3a).

In mouse lung tissue, the Singleron device achieved relatively high cell viability, although the differences were minimal. However, sTED produced a cell yield per gram of tissue that was similar to that produced by manual extraction and consistently higher than that produced by the Singleron device. Remarkably, sTED also resulted in a smaller variation in cell yield than the manual method (Fig. 3b). These findings emphasize the ability of sTED to deliver high-yield and reproducible cell extraction from soft tissues.

4.3 Primary cell extraction from ultrasmall samples

A key advantage of the proposed sTED system over existing cell extraction platforms is its ability to efficiently process ultrasmall tissue samples. We investigated this feature

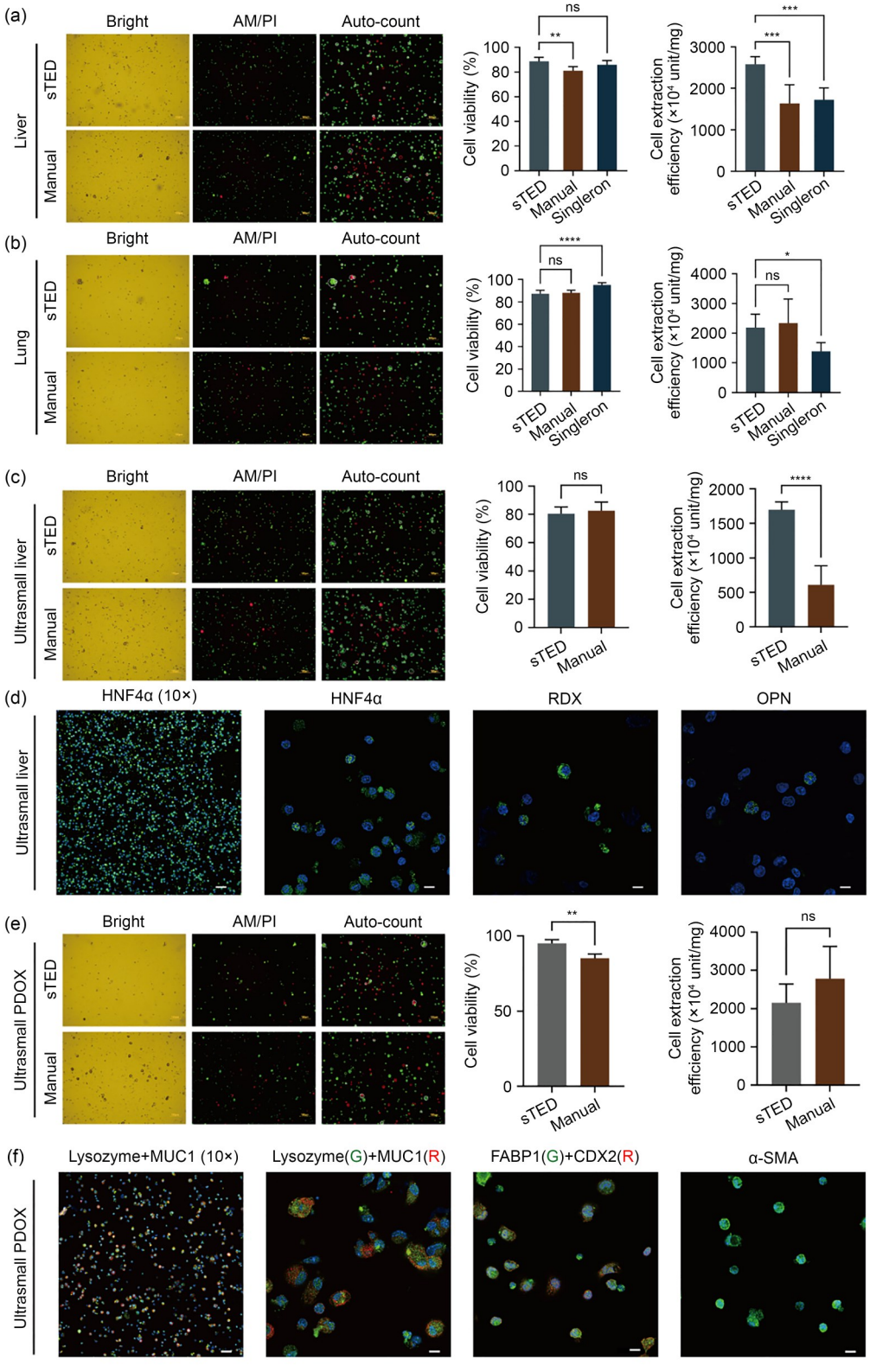

Fig. 3 Cell extraction efficiency. Comparison of sTED, manual extraction, and Singleron's PythoN system for normal mouse liver (a) and lung (b) tissues. Each subfigure includes representative images (left), cell viability assays (middle), and extraction rates per unit mass (right). Comparison of sTED and manual extraction for ultrasmall mouse liver (c) and PDOX (e) samples, with the same layout. Immunofluorescent staining of cells extracted from ultrasmall mouse liver (d) and PDOX (f) samples (G: green; R: red). Scale bars in (a, b, c, e): 50 μm for the left image, 10 μm for the others. Scale bars in (d, f): 50 μm for the left image, 20 μm for the others. Data are expressed as mean±standard deviation (n=4). $^{*}p<0.05$, $^{**}p<0.01$, $^{***}p<0.001$, and $^{****}p<0.0001$; ns: not significant

using tissue fragments weighing <0.02 g collected from mouse liver and PDOX models.

In the ultrasmall mouse liver samples, sTED achieved comparable cell viability to that of manual extraction but significantly outperformed manual extraction in terms of cell yield per unit mass. Furthermore, the proposed device demonstrated lower intergroup variability in extraction rates than the manual method (Fig. 3c).

To confirm the cell types extracted from minimal tissue, a cytocentrifugation staining method was used to label hepatocytes (hepatocyte nuclear factor 4α (HNF4α) and radixin (RDX)) and bile duct cells (osteopontin (OPN)) (Fig. 3d).

In the PDOX colorectal cancer model, sTED yielded slightly higher cell viability than manual extraction. Although the cell extraction efficiency of sTED was slightly lower than the manual method, the difference was not statistically significant (Fig. 3e). In patient-derived tumor tissues, cell viability remained above 80%, and any observed reductions were primarily attributed to tissue necrosis rather than extraction inefficiency.

For the PDOX colorectal cancer model, a cytocentrifugation staining method was used to label normal Paneth cells (lysozyme), goblet cancer cells (mucin 1 (MUC1)), normal epithelial cells (fatty acid binding protein 1 (FABP1)), cancer epithelial cells (caudal type homeobox 2 (CDX2)), and tumor fibroblasts (α-smooth muscle actin antibody (α-SMA)) (Fig. 3f).

5 Discussion

Automation via sTED reduces procedural variability and enhances reproducibility in organoid-based research. Unlike manual methods, which suffer from cell loss and inconsistency in ultrasmall samples like needle biopsies, sTED integrates mechanical dissociation and enzymatic digestion, minimizing sample loss with specialized pipette designs. While commercial systems (e.g., gentleMACS^{TM}, STEMprep^{TM}, and PythoN Junior) are suited for larger samples (>100 mg), sTED processes as little as 5 mg, yielding $1.5\times10^4 - 2.5\times10^4$ cells/mg from mouse liver with >90% viability and >60% in human tumors.

The T–S mechanism enables precise dissection within 1 min, preserving critical cell populations, such as tumor epithelial cells and fibroblasts in colorectal cancer samples, for translational organoid models. Automation eliminates the need for constant supervision, integrating seamlessly into organoid workflows and laying the groundwork for fully equipment-driven pipelines. Future enhancements will expand sTED's utility across diverse tissues and human tumor biopsies, further supporting its clinical relevance.

Supplementary Information The online version contains supplementary material available at https://doi.org/10.1631/bdm.2500186.

Acknowledgements This work was supported by the National Natural Science Foundation of China (Nos. 32371470 and 82341019) and the Department of Science and Technology of Guangdong Province (No. 2023B0909020003).

Author contributions SHM, WLW, YDC, and XYD designed the study. WLW and ZYL designed and manufactured the device. YZ provided constructive suggestions. WLW and YFW performed the experiments. WLW analyzed the data. WLW, DK, and ZTW wrote the manuscript. SHM supervised the work and revised the manuscript. All authors read and approved the final manuscript.

Declarations

Conflict of interest The authors declare that they have no conflict of interest.

Ethical approval Human samples were collected after informed written consent (including consent to participate and consent to publish) was obtained from all donors in accordance with study protocols conforming to the provisions of the Declaration of Helsinki. For the pediatric participants, written informed consent was obtained from adult legal guardians of the children before enrolment. The study was approved by the Ethics Committee of Tsinghua Shenzhen International Graduate School (Refs. 202171 and 202295).

Patient-derived colorectal cancer and liver cancer samples were obtained from Shenzhen People's Hospital, Shenzhen, China (Ethical Development No. 2024-08401).

Data availability The data that support the findings of this study are available from the corresponding author upon reasonable request.

Generative AI and AI-assisted technologies in the writing process During the preparation of this work, the authors used large language models, i.e., OpenAI's ChatGPT (GPT-4o and GPT-4omini) and Anthropic's Claude (3.7 Sonnet), to improve language and readability and to assist with generating the graphical abstract. After using these tools, the authors reviewed and edited the content as needed and take full responsibility for the content of the publication.

References

1. Geurts MH, Clevers H (2023) CRISPR engineering in organoids for gene repair and disease modelling. Nat Rev Bioeng 1(1):32–45. https://doi.org/10.1038/s44222-022-00013-5
2. Lin L, DeMartino J, Wang DS et al (2023) Unbiased transcription factor CRISPR screen identifies ZNF800 as master repressor of enteroendocrine differentiation. Science 382(6669):451–458. https://doi.org/10.1126/science.adi2246
3. Hendriks D, Brouwers JF, Hamer K et al (2023) Engineered human hepatocyte organoids enable CRISPR-based target discovery and drug screening for steatosis. Nat Biotechnol 41(11):1567–1581. https://doi.org/10.1038/s41587-023-01680-4
4. Millen R, de Kort WWB, Koomen M et al (2023) Patient-derived head and neck cancer organoids allow treatment stratification and serve as a tool for biomarker validation and identification. Med 4(5):290–310.e12. https://doi.org/10.1016/j.medj.2023.04.003
5. Ji SY, Feng L, Fu ZL et al (2023) Pharmaco-proteogenomic characterization of liver cancer organoids for precision oncology. Sci Transl Med 15(706):eadg3358. https://doi.org/10.1126/scitranslmed.adg3358
6. Polak R, Zhang ET, Kuo CJ (2024) Cancer organoids 2.0: modelling the complexity of the tumour immune microenvironment.

Nat Rev Cancer 24(8):523–539.
https://doi.org/10.1038/s41568-024-00706-6
7. Zapatero MR, Tong A, Opzoomer JW et al (2024) Trellis tree-based analysis reveals stromal regulation of patient-derived organoid drug responses. Cell 187(25):7335–7349.
https://doi.org/10.1016/j.cell.2024.11.023
8. Bose S, Clevers H, Shen XL (2021) Promises and challenges of organoid-guided precision medicine. Med 2(9):1011–1026.
https://doi.org/10.1016/j.medj.2021.08.005
9. Zheng YC, Han F, Wu ZY et al (2024) MAIT cell activation and recruitment in inflammation and tissue damage in acute appendicitis. Sci Adv 10(24):eadn6331.
https://doi.org/10.1126/sciadv.adn6331
10. Salahudeen AA, Seoane JA, Yuki K et al (2023) Functional screening of amplification outlier oncogenes in organoid models of early tumorigenesis. Cell Rep 42(11):113355.
https://doi.org/10.1016/j.celrep.2023.113355
11. Hu WX, Lazar MA (2022) Modelling metabolic diseases and drug response using stem cells and organoids. Nat Rev Endocrinol 18(12):744–759.
https://doi.org/10.1038/s41574-022-00733-z
12. Zheng YC, Tian QY, Yang HW et al (2025) Identification of nicotinic acetylcholine receptor for N-acetylcysteine to rescue nicotine-induced injury using beating cilia in primary tissue derived airway organoids. Adv Sci 12(1):2407054.
https://doi.org/10.1002/advs.202407054
13. Tadokoro T, Murata S, Kato M et al (2024) Human iPSC-liver organoid transplantation reduces fibrosis through immunomodulation. Sci Transl Med 16(757):eadg0338.
https://doi.org/10.1126/scitranslmed.adg0338
14. Zhao YM, Landau S, Okhovatian S et al (2024) Integrating organoids and organ-on-a-chip devices. Nat Rev Bioeng 2(7):588–608.
https://doi.org/10.1038/s44222-024-00207-z
15. Hendijani F (2017) Explant culture: an advantageous method for isolation of mesenchymal stem cells from human tissues. Cell Prolif 50(2):e12334.
https://doi.org/10.1111/cpr.12334
16. Lulevich V, Zink T, Chen HY et al (2006) Cell mechanics using atomic force microscopy-based single-cell compression. Langmuir 22(19):8151–8155.
https://doi.org/10.1021/la060561p
17. Kudo T, Meireles AM, Moncada R et al (2024) Multiplexed, image-based pooled screens in primary cells and tissues with PerturbView. Nat Biotechnol (early access).
https://doi.org/10.1038/s41587-024-02391-0
18. Gesualdo L, Fiorentino M, Conserva F et al (2024) Should we enlarge the indication for kidney biopsy in patients with diabetes? The pro part. Clin Kidney J 17(1):sfad266.
https://doi.org/10.1093/ckj/sfad266
19. El Sissy C, Kirilovsky A, Pagès CL et al (2024) International validation of the immunoscore biopsy in patients with rectal cancer managed by a watch-and-wait strategy. J Clin Oncol 42(1):70–80.
https://doi.org/10.1200/jco.23.00586